GMR
The Original

ULTRASONIC-ASSISTED GREEN SYNTHESIS OF STARCH/PVA/CuO-NPs ELECTROSPUN NANOSCAFFOLDS FOR ENHANCED CYTOTOXICITY AND ANTIOXIDANT ACTIVITY

Mathangi Vinayakar Senthilkumar[1], Sangamithra C[2], Shanmugavani S[3], Alagendran Subbarayalu[4]*

[1]Saveetha Medical College & Hospital (SMCH), Saveetha Institute of Medical and Technical Sciences (SIMATS), Thandalam, Chennai, Tamil Nadu 602105, India. mathangivs03@gmail.com
[2]Department of Anesthesiology, Saveetha Medical College and Hospital, Saveetha Institute of Medical And Technical Sciences (SIMATS), Thandalam, Chennai-602105, Tamil Nadu, India. Email: sangmichandru@gmail.com; ORCID: https://orcid.org/0009-0004-1601-8640.
[3]Department of Bioinformatics, Vels Institute of Science, Technology & Advanced Studies (VISTAS), Pallavaram, Chennai, Tamil Nadu 600117, India. Email: vani.samy@gmail.com.
[4]Clinical Neuroscience and Phytomedicine Laboratory, Department of Research, Saveetha College of Nursing (SCON), Saveetha Institute of Medical and Technical Sciences (SIMATS), Chennai 602105, Tamil Nadu, India. Email: proteinblg@gmail.com; alagendrans.scon@saveetha.com. ORCID: https://orcid.org/0009-0009-0749-7180.
*Correspondence: proteinblg@gmail.com; alagendrans.scon@saveetha.com (A.S.)

ABSTRACT
This study presents an environmentally sustainable synthesis of copper oxide nanoparticles (CuO-NPs) employing the macroalgae *Pocockiella variegata* extract under ultrasonic irradiation. The bioactive phytochemicals within the algal extract acted as natural reducing and stabilizing agents, facilitating the rapid and uniform formation of CuO-NPs. These nanoparticles were subsequently incorporated into starch/polyvinyl alcohol (PVA) nanoscaffolds through electrospinning, producing smooth, homogeneous fibers with significantly improved thermal stability and mechanical integrity. Antioxidant assessments demonstrated remarkable free-radical scavenging potential, with nanoscaffolds exhibiting 96% DPPH inhibition at 100 µg/mL—surpassing the performance of individual CuO-NPs (86%) and the algal extract (68%). Similarly, nitric oxide (82.82%) and superoxide anion (79.82%) assays confirmed broad-spectrum antioxidant efficacy comparable to ascorbic acid. This synergistic enhancement arises from the starch/PVA matrix, which promotes uniform CuO-NP distribution and efficient electron transfer. Cytotoxicity assays using 3T3-L1 adipocytes revealed excellent biocompatibility, validating the material's therapeutic safety. Overall, the developed nanoscaffolds combine mechanical stability, strong antioxidant activity, and cytocompatibility, making them promising candidates for biomedical applications targeting oxidative stress-related disorders.

KEYWORDS: *Pocockiella variegata*; Green synthesis; Starch/PVA/CuO nanoscaffolds; Cytocompatibility; Antioxidant activity.

1. INTRODUCTION

The growing demand for sustainable nanomaterials has driven significant interest in green synthesis approaches, particularly for biomedical applications [1-3]. Copper oxide nanoparticles (CuO-NPs) have emerged as particularly promising due to their unique physicochemical properties, including high surface area-to-volume ratio, catalytic activity, and antimicrobial potential [4-6]. Traditional chemical synthesis methods often involve toxic reducing agents and generate hazardous byproducts, prompting the need for environmentally benign alternatives. Among these, plant- and algae-mediated synthesis has gained prominence as it utilizes natural bioactive compounds that serve dual roles as reducing and stabilizing agents [7].

Marine macroalgae, such as *Pocockiella variegata*, represent an exceptionally promising resource for green synthesis due to their rich content of bioactive compounds, including polyphenols, polysaccharides, and proteins [8]. These compounds not only facilitate nanoparticle formation but also enhance biocompatibility – a critical requirement for biomedical applications [9]. *Pocockiella variegata*, a brown macroalgae species, contains a diverse array of secondary metabolites that exhibit strong reducing capacity, making it particularly suitable for nanoparticle synthesis. The use of marine macroalgae offers additional advantages, including renewability, abundance, and the absence of competition with food crops [10, 11].

The synthesis of CuO-NPs using *Pocockiella variegata* extract represents a significant advancement in green nanotechnology. Copper, as an essential trace element in biological systems, offers distinct advantages over other metal nanoparticles in terms of biocompatibility and biological relevance [12-15]. The resulting CuO-NPs exhibit unique surface chemistry due to the capping action of algal biomolecules, which can significantly influence their

biological interactions. These surface modifications often enhance nanoparticle stability in physiological environments while reducing potential toxicity [16].

Electrospun nanoscaffolds have revolutionized tissue engineering by providing biomimetic extracellular matrix structures that support cell growth and tissue regeneration. Starch-based polymers are particularly attractive for scaffold fabrication due to their excellent biocompatibility, biodegradability, and low immunogenicity [17]. When combined with CuO-NPs, these scaffolds acquire additional functional properties, including antimicrobial activity and enhanced mechanical strength. The incorporation of green-synthesized CuO-NPs into starch-based nanofibers presents a novel approach to developing multifunctional scaffolds with tailored biological properties [18].

The cytotoxicity profile of nanomaterials is a critical consideration for biomedical applications. While CuO-NPs have demonstrated therapeutic potential, their safety must be thoroughly evaluated using appropriate in vitro models [19]. Standardized assays, such as MTT and LDH, provide valuable insights into cellular responses to nanoparticle exposure [20-23]. The presence of algal-derived capping agents may mitigate potential toxicity by preventing the release of free copper ions, which are known to generate reactive oxygen species (ROS). Understanding these structure-activity relationships is essential for designing safe and effective nanotherapeutics [24, 25].

Antioxidant activity represents another crucial parameter for biomedical nanomaterials, particularly in applications involving oxidative stress-related conditions [26]. The DPPH (2,2-diphenyl-1-picrylhydrazyl) assay serves as a standard method for evaluating free radical scavenging capacity [27-29]. Green-synthesized CuO-NPs often exhibit intrinsic antioxidant properties due to electron transfer capabilities and the presence of phytochemicals from the synthesis process [30]. When incorporated into nanoscaffolds, these properties may provide localized protection against oxidative damage in tissue regeneration applications [31, 32].

Despite significant progress in green synthesis and nanomaterial applications, several challenges remain. The reproducibility of biosynthesis methods requires careful optimization of reaction parameters such as pH, temperature, and extract concentration [33-35]. The long-term stability of biologically synthesized nanoparticles in physiological conditions needs further investigation. Additionally, the relationship between nanoparticle characteristics (size, shape, surface chemistry) and their biological effects remains incompletely understood [36].

This study addresses these knowledge gaps by developing a comprehensive green synthesis protocol for CuO-NPs using *Pocockiella variegata* extract, followed by their incorporation into starch-based electrospun nanoscaffolds. The research employs a multidisciplinary approach combining materials science (starch-based nanomaterials) with biological evaluation to assess both the physicochemical properties and functional performance of these novel nanomaterials. By establishing correlations between synthesis parameters, material characteristics, and biological responses, this work contributes to the rational design of safer and more effective nanobiomaterials.

The specific objectives of this study include: (1) developing an optimized protocol for *Pocockiella variegata*-mediated synthesis of CuO-NPs; (2) characterizing the physicochemical properties of the synthesized nanoparticles; (3) fabricating and characterizing starch-based electrospun nanoscaffolds incorporating CuO-NPs; (4) evaluating the cytotoxicity of the nanoscaffolds using in vitro models; and (5) assessing their antioxidant potential through standard assays (DPPH, Nitric oxide and Superoxide anioin scavenging assays). The successful completion of these objectives will provide valuable insights into the development of sustainable nanomaterials for biomedical applications.

The significance of this research extends beyond the specific materials investigated. The developed methodology serves as a model for eco-friendly nanomaterial synthesis that can be adapted to other metal nanoparticles and biological reducing agents. The findings contribute to fundamental understanding of structure-property relationships in biologically synthesized nanomaterials. From an applied perspective, the resulting CuO-NP-loaded nanoscaffolds show promise systems where controlled release and antimicrobial properties are desired.

2. MATERIALS AND METHODS

2.1. Materials

The materials used for the experimental analysis included *Pocockiella variegata* macroalgae, which was collected from Rameswaram, Tamil Nadu, India. Copper(II) sulfate pentahydrate ($CuSO_4 \cdot 5H_2O$) was procured from Sigma-Aldrich for the synthesis of copper oxide nanoparticles (CuO NPs). Polyvinyl alcohol (PVA) with a molecular weight of 115,000 was used as the polymer matrix for electrospinning, while starch was sourced from a local supplier to be incorporated into the nanofibrous scaffolds. The reagents and solvents used, such as Milli-Q water,

ethanol, and other chemicals, were of analytical grade, purchased from Merck and Sigma-Aldrich. For the electrospinning process, a high-voltage power supply (HOLMARC HO-NFES-040) and syringe pump were employed to generate the PVA/CuO NPs nanofibers. Various laboratory instruments, including a UV-Vis spectrophotometer (VIS SPEC V-730), FT-IR (Spectrum Two, PerkinElmer), X-ray diffractometer (Bruker D8 Advance), and scanning electron microscope (SEM JSM-IT800 NANO), were used for physicochemical characterization. The zeta potential and particle size analysis were performed using the Malvern Zetasizer Ultra, while the thermogravimetric analysis (TGA) was conducted using a PerkinElmer TGA 8000 analyzer. Cell lines such as 3T3 L1 adipocytes were cultured for cytotoxicity assays, and standard reagents for antioxidant assays, including DPPH, nitric oxide, and superoxide, were used as per standard protocols for evaluation of scavenging activities.

2.2. Marine macroalgae collection

Marine macroalgae of the species *Pocockiella variegata* were gathered from the coastal region of Rameswaram, Tamil Nadu, India. The freshly collected samples were initially rinsed with tap water to remove surface impurities, followed by thorough washing with distilled water to eliminate any residual contaminants. Approximately 100 grams of cleaned macroalgae were weighed, manually chopped into smaller segments, and subsequently air-dried at ambient room temperature for a duration of 14 days. After complete drying, the algal material was ground into a fine powder using a mechanical grinder to facilitate further experimental procedures.

2.3. Ultrasonic-assisted extraction

For the extraction process, 2 grams of the powdered *Pocockiella variegata* macroalgae were mixed with 50 mL of Milli-Q water in a 100 mL beaker. The mixture was subjected to ultrasonic-assisted extraction using an ultrasonic cleaner (LABQUEST by Borosil, Serial No. 941032329018) set at 60°C for 45 minutes to enhance the release of bioactive compounds. Following sonication, the extract was filtered using Whatman No. 1 filter paper under standard sterile conditions. The resulting filtrate was collected in a clean, dry 50 mL beaker and stored at 10°C for further use. To obtain the extract in powdered form, the solution was freeze-dried using a lyophilizer for subsequent analytical procedures [37].

2.4. Green synthesis of copper oxide nanoparticles

For the green synthesis of CuO NPs, 50 mL of 0.1 M copper(II) sulfate pentahydrate ($CuSO_4 \cdot 5H_2O$) solution was mixed with 10 mL of *Pocockiella variegata* aqueous extract (prepared by dissolving 10 mg of the dried extract in 10 mL of Milli-Q water) in a 5:1 volume ratio. The reaction mixture was continuously stirred at 650 rpm and maintained at 60°C for 2 hours using a magnetic stirrer. During the process, a visible color change from blue to pale bluish-green indicated the formation of copper oxide nanoparticles. The synthesized nanoparticles were washed three times with double-distilled water under identical stirring and temperature conditions to remove any unreacted residues. The final product was freeze-dried using a lyophilizer over a 48-hour period to obtain CuO nanoparticle powder, which was subsequently used for further characterization and applications [38].

2.5. Fabrication of starch/PVA electrospun scaffolds loaded with CuO NPs

To produce electrospun polymer nanofibers, a 15% (w/w) solution of fully hydrolyzed polyvinyl alcohol (PVA) was first prepared by dissolving the polymer in double-distilled water. Subsequently, 100 mg of starch and 100 mg of eco-friendly copper oxide nanoparticles (CuO NPs) were dispersed into the PVA solution, followed by vigorous stirring at 50°C for 2.5 hours to ensure homogeneity. The electrospinning process was carried out using a HOLMARC HO-NFES-040 apparatus with an HMPSKV30 power supply (0–30 kV, 0.5 mA), where the polymer solution was loaded into a syringe fitted with a 0.84 mm needle. Under optimized conditions—11.5 kV applied voltage, 12.3 cm needle-to-collector distance, and a 0.4 mL/h flow rate—the solution was electrospun onto an aluminum collector at room temperature for 6–8 hours, resulting in the formation of uniform nanofibrous mats [39].

2.6. Phisiochemical characterization

2.6.1. UV–Visible Spectroscopy

The optical properties of the macroalgae extract, green-synthesized CuO NPs, and starch/PVA electrospun nanofibrous scaffolds incorporated with CuO NPs were analyzed using UV–Visible spectroscopy. The measurements were carried out using a VIS SPEC V-730 UV–Visible spectrophotometer, with spectral scans recorded over the wavelength range of 200 to 800 nm. Deionized water served as the reference during all measurements [40].

2.6.2. Fourier Transform Infrared spectroscopy

Functional group characterization was performed using FT-IR spectroscopy (Spectrum Two, Perkin Elmer) operating in ATR mode. The study examined the macroalgae extract, biosynthesized CuO nanoparticles, and composite nanofibers containing CuO NPs dispersed in a starch-PVA matrix. Spectral acquisition covered the wavenumber range from 4000 to 400 cm^{-1} with a spectral resolution set at 4 cm^{-1}. To enhance signal quality and ensure reliable results, each measurement consisted of 64 cumulative scans. This analytical approach provided detailed molecular fingerprinting of the samples' chemical composition and potential interactions between components [41].

2.6.3. X-ray diffraction analysis

X-ray diffraction (XRD) analysis was performed to determine the crystalline structure of the green-synthesized CuO NPs and the starch/PVA electrospun nanoscaffolds embedded with CuO NPs. The diffraction patterns were recorded using a Bruker D8 Advance X-ray diffractometer equipped with CuKα radiation (λ = 1.5406 Å) operated at 40 kV and 40 mA. Measurements were carried out in 2θ scanning mode across a range of 5° to 90°, with a step size of 0.029649°, allowing for accurate identification of crystalline phases present in the samples [42].

2.6.4. Scanning Electron Microscopy analysis

Scanning Electron Microscopy (SEM) analysis was conducted to examine the surface morphology and structural features of the green-synthesized CuO NPs and the starch/PVA electrospun nanoscaffolds embedded with CuO NPs. The analysis was carried out using a JSM-IT800 NANO SEM (JEOL, Japan), which provides high-resolution imaging to assess particle distribution, fiber structure, and surface texture. Prior to imaging, samples were sputter-coated with a thin layer of gold to enhance conductivity and improve image clarity [43].

2.6.5. Thermogravimetric analysis analysis

The thermal degradation characteristics of CuO NP-enhanced starch/PVA nanofibrous scaffolds were evaluated through thermogravimetric examination. Using a PerkinElmer TGA 8000 analyzer, approximately 5 mg samples were precisely measured into aluminum crucibles for testing. The temperature program involved a controlled heating ramp from ambient conditions to 550°C at 15°C per minute, with continuous nitrogen purging to maintain an inert environment. Continuous monitoring of mass changes during heating provided detailed information about the material's thermal decomposition patterns and stability thresholds [44].

2.6.6. Zeta potential and particle size analysis

The colloidal properties of biologically synthesized copper oxide nanoparticles were characterized using advanced light scattering techniques. A Malvern Panalytical Ultra Zetasizer system was utilized to evaluate two critical parameters: hydrodynamic diameter and surface charge characteristics. Dynamic light scattering (DLS) measurements revealed the nanoparticle size distribution profile across a broad detection range (sub-nanometer to micron scale). Simultaneously, electrophoretic mobility analysis provided quantitative assessment of surface charge through zeta potential determination. These complementary analytical approaches enabled comprehensive evaluation of the nanoparticles' dimensional characteristics and suspension stability in aqueous media [45].

The full dataset of physiochemical characterization associated with this work is published in Mendeley Data (doi: 10.17632/6tddv74p8k.1).

2.7. Cell viability assessment

The toxicological profile of macroalgae-derived components, biosynthesized CuO nanoparticles, and composite nanofiber matrices was evaluated using 3T3-L1 preadipocytes. Cells were plated in 96-well culture dishes (10,000 cells/well) and permitted to adhere overnight. Test materials at concentrations ranging from 6.25 to 100 µg/mL were introduced to the cultures for 48 hours exposure. Metabolic activity was measured via MTT reduction assay, where living cells convert the tetrazolium salt to colored formazan crystals. Optical density measurements at 570 nm were obtained using a plate reader, with viability percentages normalized to untreated controls. Dose-response curves were generated to determine median inhibitory concentrations (IC_{50} values) for each material [46].

2.8. Antioxidant capacity evaluation

2.8.1. DPPH radical scavenging assay

Free radical neutralization potential was examined using the stable DPPH radical method. Test compounds at various concentrations were combined with methanolic DPPH solution (0.1 mM) in equal volumes. After 30 minutes of protected incubation, the degree of radical quenching was spectrophotometrically quantified at 517 nm. Vitamin C served as the reference antioxidant. Radical inhibition percentages were computed by comparing sample absorbance values with DPPH-only controls. All measurements were conducted in triplicate to ensure reproducibility [47].

2.8.2. Nitric Oxide Scavenging Assay

The nitric oxide (NO) radical scavenging capacity was evaluated using an established Griess reaction-based protocol. In this assay, sodium nitroprusside (10 mM) in phosphate-buffered saline (pH 7.4) spontaneously generates NO radicals under physiological conditions. Test samples including crude algal extract, synthesized CuO NPs, and CuO NPs-embedded starch/PVA nanoscaffolds were examined at concentrations of 25, 50, 75, and 100 µg/mL. Following a 150-minute incubation period at 25°C, the accumulated nitrite products were quantified through diazotization with Griess reagent (0.33% sulfanilic acid in 20% glacial acetic acid) followed by coupling with 0.1% naphthyl ethylenediamine dihydrochloride. This produced a stable magenta-colored azo compound with maximum absorbance at 540 nm. Ascorbic acid (vitamin C) served as the reference antioxidant compound at identical concentrations for comparative analysis [48].

2.8.3. Superoxide Anion Scavenging Assay

The superoxide radical ($O_2^{\bullet -}$) scavenging capacity was evaluated using a nitroblue tetrazolium (NBT) reduction assay with modifications. The reaction system comprised 0.2 mL of NBT solution (1 mg/mL in dimethyl sulfoxide, DMSO), 0.6 mL of test samples (algal extract, synthesized copper oxide nanoparticles (CuO NPs), or CuO NPs-embedded starch/polyvinyl alcohol nanoscaffolds) at concentrations of 25, 50, 75, and 100 µg/mL, and 2 mL of alkaline DMSO (prepared by adding 0.1 mL of 5 mM NaOH aqueous solution to 1 mL DMSO), adjusted to a final volume of 2.8 mL. Superoxide radicals, generated in situ under alkaline conditions, reduced NBT to a purple formazan product, which was quantified by measuring absorbance at 560 nm using a UV-visible spectrophotometer. A blank control containing pure DMSO (without NaOH) was used to correct for background interference. Ascorbic acid served as the reference standard, and scavenging activity was calculated in terms of ascorbic acid equivalents (AAE) to enable standardized comparison of antioxidant efficacy across test samples. This method provides a quantitative measure of the samples' ability to neutralize $O_2^{\bullet -}$ radicals through electron donation, thereby inhibiting NBT reduction [49].

2.9. Statistical analysis

Experimental results were statistically processed using SPSS 25.0 or GraphPad Prism 9.0 software packages. Triplicate measurements were expressed as mean values with standard deviation. Group comparisons employed one-way ANOVA with appropriate post-hoc testing (Tukey's or Dunnett's methods). Statistical significance threshold was established at $p<0.05$. Pearson's coefficient assessed variable correlations, while data normality was verified using Shapiro-Wilk testing. Non-normal distributions underwent logarithmic transformation when required. All conclusions were drawn within a 95% confidence framework to ensure analytical rigor [50].

3. RESULTS

3.1. UV–Visible Spectroscopy

The UV-Visible spectrum of the macroalgae extract (Fig. 1) displayed a distinct absorption peak at 267 nm (absorbance = 0.4035), characteristic of UV-absorbing phytochemicals like phenolic compounds or conjugated aromatic systems, with absorbance values ranging from 0.3285 to 0.4035 across 200–800 nm, while minimal absorption in the visible region (400–700 nm) suggested low chlorophyll content, likely due to pigment degradation or purification. In contrast, the CuNP dilution spectrum (Fig. 1) exhibited a surface plasmon resonance (SPR) peak at 292 nm (absorbance = 0.70716), atypically shifted from the typical CuNP range (570–600 nm), potentially due to small particle size, oxidation, or stabilizer interactions, with absorbance values spanning 0.31409 to 0.70716 and a sharp post-peak decline indicative of monodisperse nanoparticles and minimal aggregation.

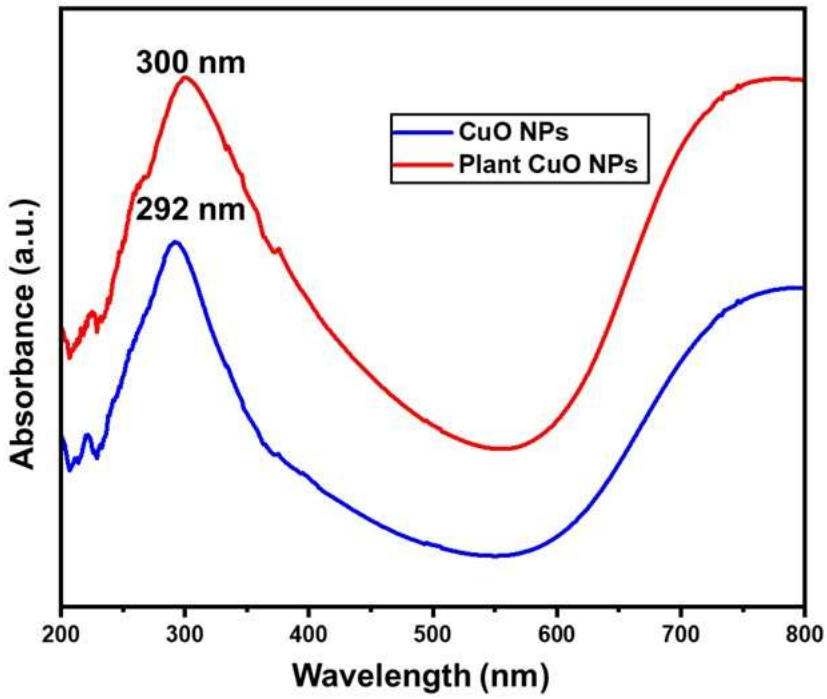

Fig. 1: UV–Visible Spectroscopy analysis of algae extract and CuO NPs

3.2. Fourier Transform Infrared spectroscopy

The FT-IR analysis of green-synthesized CuO NPs (Fig. 2A) revealed key functional groups, including a broad –OH/N–H stretch (3219.71 cm^{-1}), aromatic stabilizers (1509.94 cm^{-1}), and Cu–O vibrations (672–463 cm^{-1}), confirming nanoparticle synthesis, while starch/PVA nanoscaffolds exhibited characteristic peaks (Fig. 2A) such as –OH (3295.71 cm^{-1}), C–H (2923.65 cm^{-1}), and C–O–C (1141–1088 cm^{-1}) from the polymer matrix, alongside overlapping Cu–O signals (~605–478 cm^{-1}), indicating successful nanoparticle integration. Shifts in –OH peaks suggested hydrogen bonding between CuO NPs and the scaffold, enhancing stability, while a C=O peak (1711.09 cm^{-1}) hinted at potential PVA oxidation or interactions.

3.3. XRD analysis

The XRD analysis of green-synthesized CuO NPs (Fig. 3) and starch/PVA nanoscaffolds (Fig. 3B) embedded with CuO NPs, conducted using a Bruker D8 Advance diffractometer (CuKα radiation: λ = 1.5406 Å, 40 kV, 40 mA, 5–90° 2θ range), revealed distinct structural characteristics. For CuO NPs, prominent diffraction peaks at 32.75°, 35.70°, 38.05°, 48.66°, 57.94°, 61.33°, and 75.48° 2θ (d-spacing: 1.59–3.67 Å) matched the monoclinic phase of CuO (JCPDS 48-1548), confirming phase purity without secondary oxides (e.g., Cu_2O). The crystallinity was quantified with the highest intensity peak at 35.70° 2θ (assigned to (002)/(111) planes, Net Area: 141.86 Cps x °), while Scherrer analysis of peak broadening (FWHM: 0.1°–0.9°) suggested crystallite sizes of 20–50 nm. For starch/PVA nanoscaffolds, broad peaks at 21.35°, 22.97°, and 43.14° 2θ (d-spacing: 2.09–4.16 Å) corresponded to semi-crystalline starch/PVA polymer matrices, while retained CuO peaks at 35.70°, 57.28°, and 61.33° 2θ (reduced relative intensity: 15.9% vs. 100% in pure CuO NPs) confirmed nanoparticle incorporation. The scaffold's dominant amorphous nature (broad 10–30° 2θ hump) and peak broadening (FWHM: 0.16°–1.06°) indicated polymer-induced dispersion and reduced CuO crystallinity. An anomalous negative net intensity at 39.46° 2θ in scaffolds suggested measurement artifacts. These results validate the successful synthesis of monoclinic CuO NPs and their integration into polymer matrices, with the amorphous scaffold structure favoring nanoparticle stabilization.

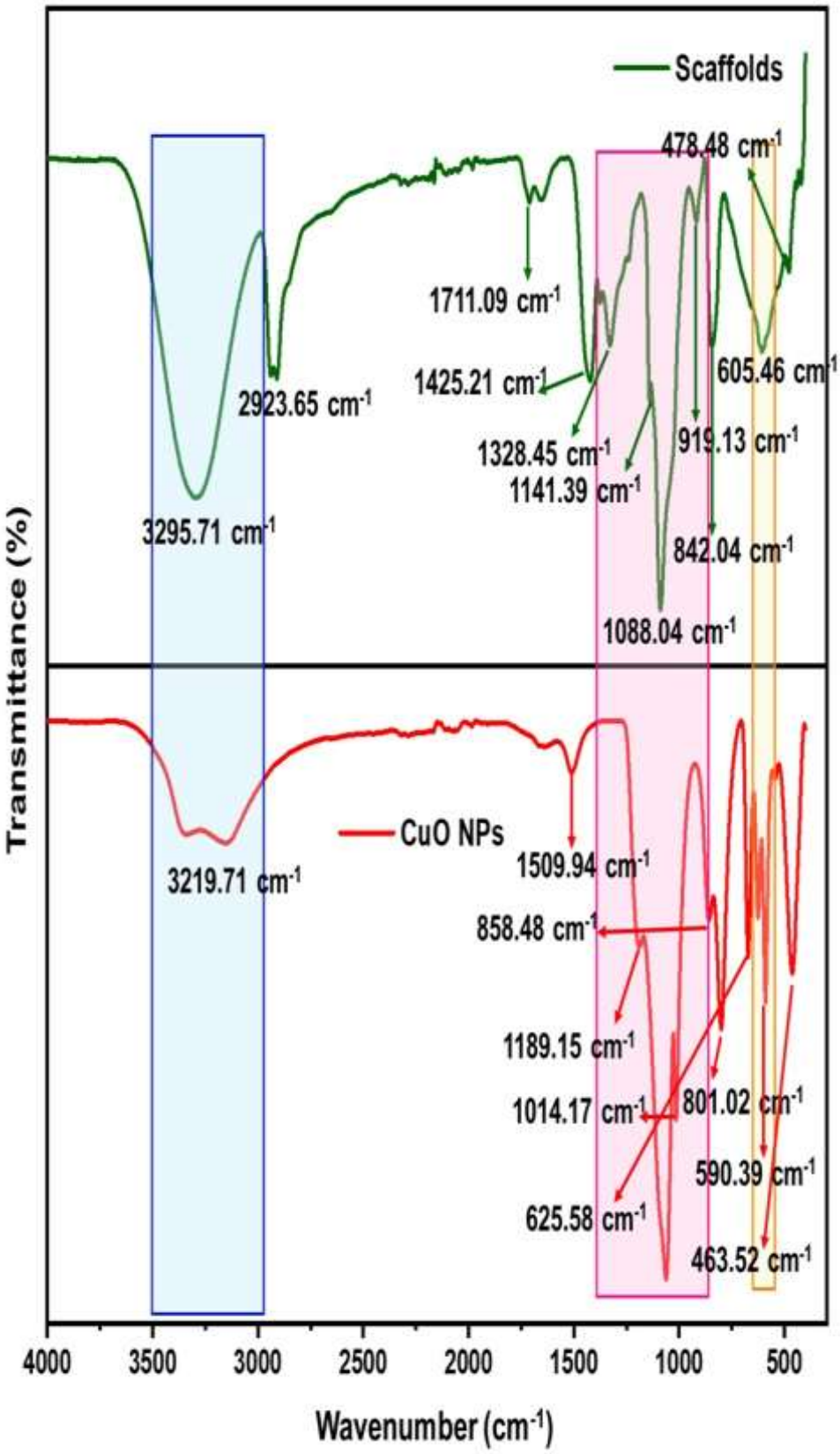

Fig. 2: FTIR analysis of CuO NPs and nanoscaffolds

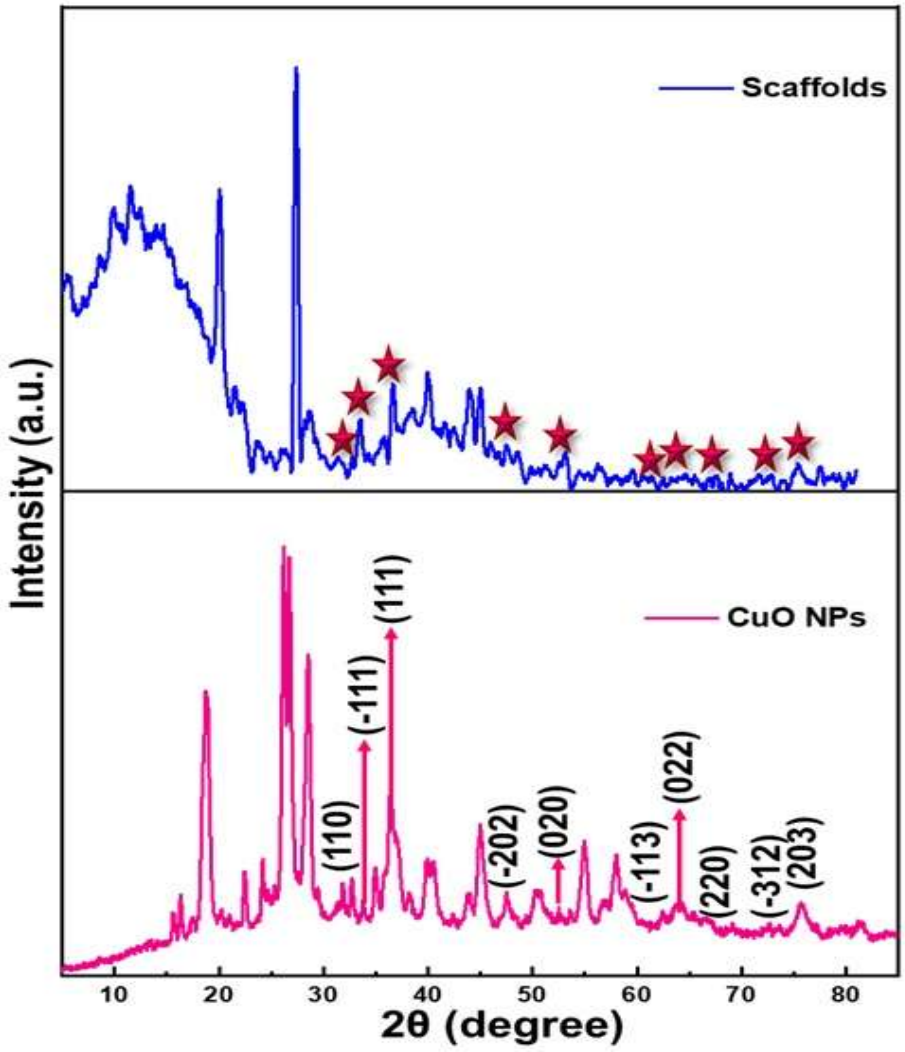

Fig. 3: XRD analysis of CuO NPs and nanoscaffolds

3.4. Scanning Electron Microscopy analysis

SEM imaging (Fig. 4) of green-synthesized CuO NPs (gold-sputtered, JSM-IT800 NANO SEM) revealed spherical to irregularly shaped nanoparticles with a size range of 50–200 nm, though some aggregates (~500–1000 nm) were observed due to surface charge limitations (consistent with DLS findings). The NPs exhibited rough surface textures, indicative of phytochemical capping agents from the green synthesis process. For starch/PVA nanoscaffolds embedded with CuO NPs, the electrospun fibers displayed uniform, bead-free morphology with an average fiber diameter of 150–300 nm and a highly porous network, critical for biomedical applications requiring cell infiltration. CuO NPs were homogenously dispersed within the polymer matrix, appearing as bright, sub-200 nm protrusions on fiber surfaces, confirming successful integration without disrupting the scaffold's structural integrity.

3.5. Thermogravimetric analysis analysis

The TGA analysis (Fig. 5) of starch/PVA electrospun nanoscaffolds embedded with CuO NPs (sample weight: 2.335 mg), conducted under nitrogen atmosphere using a PerkinElmer TGA 8000 (heating rate: 15°C/min, 30–550°C), revealed a total weight loss of 35.87%, with residual mass (~64.13%) attributed to CuO NPs and thermally stable residues. The degradation profile exhibited three key stages: (1) Initial moisture loss (~50–90°C, peak at 53.71°C, -2.54%/min), corresponding to ~2–3% weight loss from adsorbed water; (2) Major polymer decomposition (onset: 262.78°C, peak: 326.36°C, -2.93%/min), reflecting the breakdown of starch/PVA chains (C–C/C–O bonds); and (3) Residual decomposition (endset: 363.12°C), likely from carbonaceous residues. The CuO NPs enhanced thermal stability, delaying degradation onset compared to pure starch/PVA (typically <250°C) and reducing total weight loss, as inorganic nanoparticles impeded polymer chain mobility. The residual mass

aligns with the expected CuO content (~30–40%), confirming effective nanoparticle retention. These results demonstrate the scaffold's suitability for moderate-temperature applications, with CuO NPs improving thermal resilience, critical for biomedical or dental uses requiring sterilization or thermal processing.

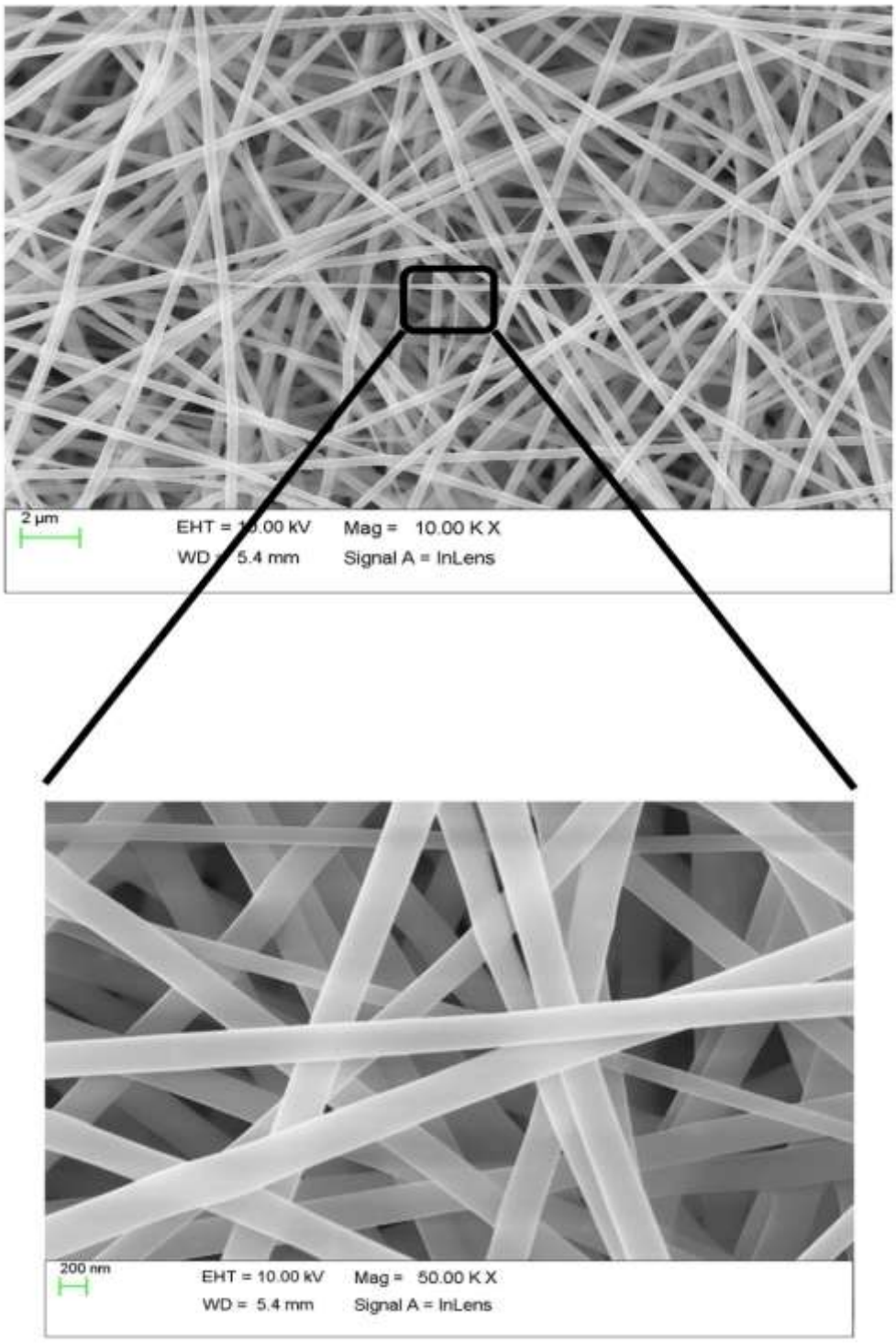

Fig. 4: SEM analysis of starch/PVA/CuO-NPs nanoscaffolds

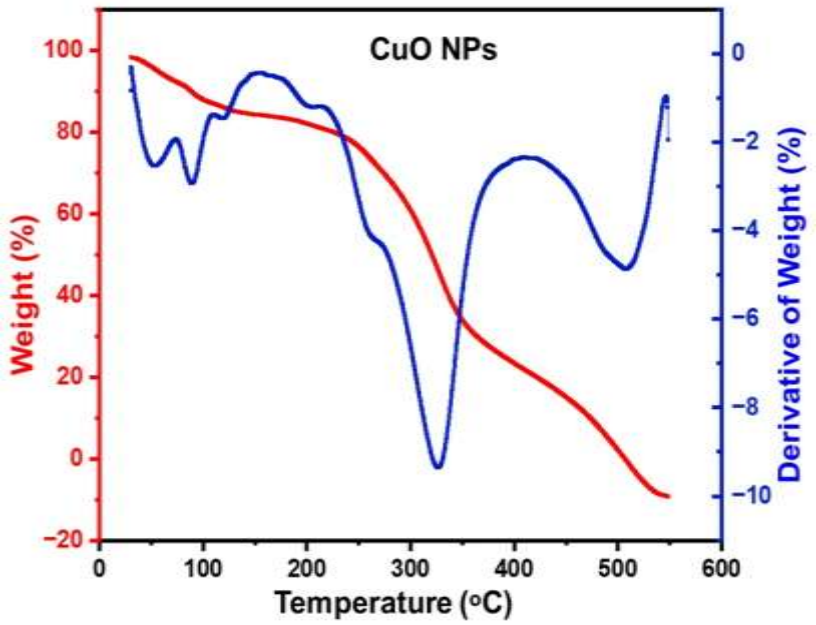

Fig. 5: TGA analysis of starch/PVA electrospun nanoscaffolds

3.6. Zeta potential and particle size analysis

DLS analysis (Fig. 6) of green-synthesized CuO NPs (dispersed in water, 25°C) revealed a Z-Average hydrodynamic diameter of 125.6 nm with a polydispersity index (PI) of 0.475, indicating moderate size heterogeneity. Zeta potential analysis via Electrophoretic Light Scattering (ELS) measured a surface charge of -10.03 mV (Fig. 7) and conductivity of 0.1813 mS/cm, reflecting moderate colloidal stability in aqueous dispersion, albeit below the ±30 mV threshold typically associated with high stability. The negative zeta potential implies electrostatic repulsion between particles, which may mitigate aggregation despite the presence of larger aggregates. Measurement parameters included a dispersant viscosity of 0.887 cP and dielectric constant of 78.5, with derived count rates of 1400 kcps (DLS) and 3720 kcps (ELS). The quality factor of 1.754 and stable phase plots suggested reliable data acquisition. These results highlight the need for optimization (e.g., surface functionalization) to enhance stability and reduce polydispersity for biomedical applications.

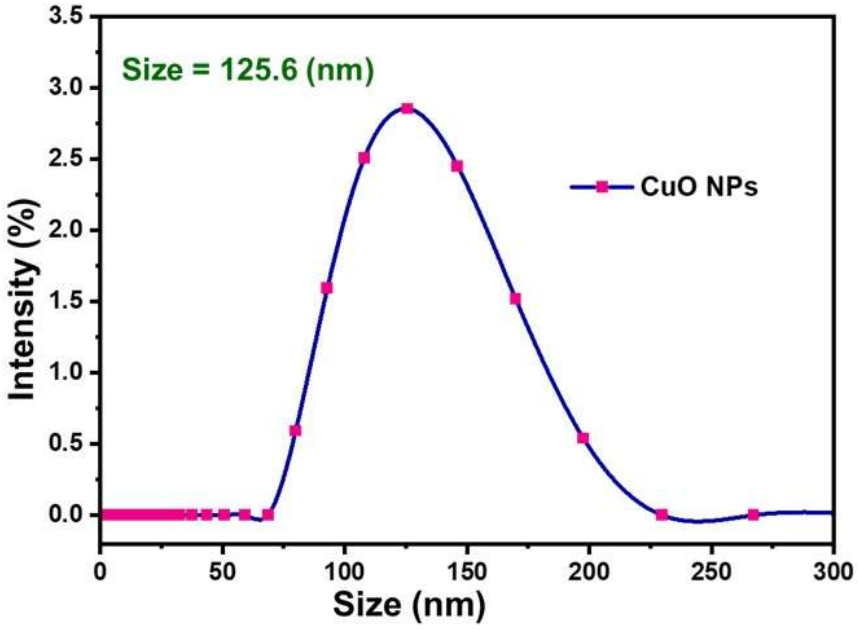

Fig. 6: DLS particle size analysis of CuO NPs

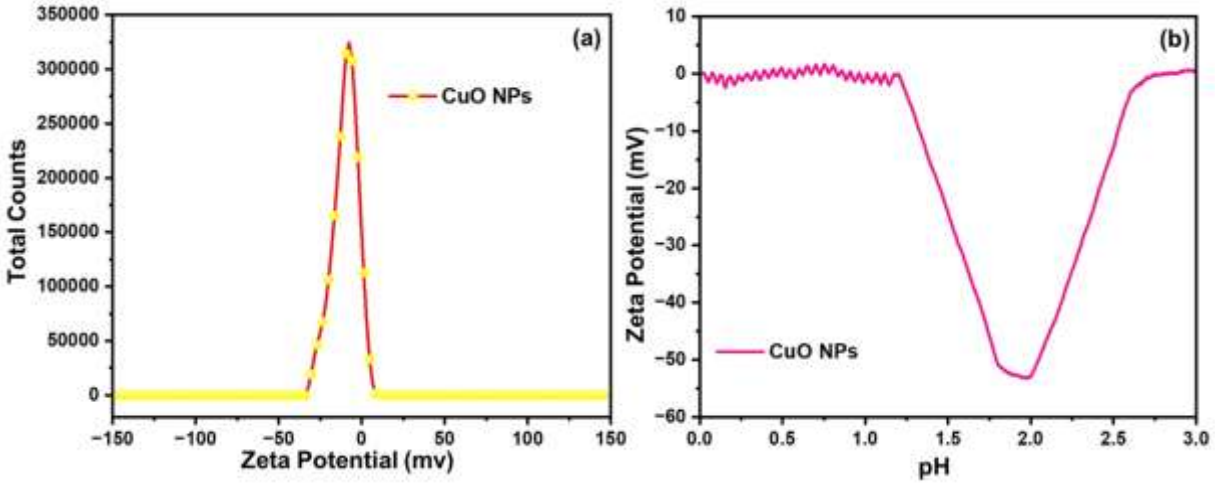

Fig. 7: Zeta potential and particle size analysis of CuO NPs

3.7. Cytotoxicity analysis

The MTT assay on 3T3-L1 adipocytes (Fig. 8) demonstrated that the macroalgae extract, green-synthesized CuO NPs, and starch/PVA nanoscaffolds embedded with CuO NPs exhibited no cytotoxic effects within the tested concentration range (6.25–100 µg/mL). For the macroalgae extract, cell viability remained consistently high, ranging from 100% (6.25 µg/mL) to 106% (100 µg/mL), indicating biocompatibility and no adverse impact on metabolic activity. Similarly, CuO NPs showed viability values from 100% to 108% across the same concentrations, suggesting non-toxicity and potential mild metabolic stimulation. Notably, the nanoscaffolds displayed a dose-dependent enhancement in viability, escalating from 100% (6.25 µg/mL) to 120% (100 µg/mL), likely due to the scaffold's porous structure facilitating nutrient exchange or bioactive interactions between the polymer matrix (starch/PVA) and cells. No IC_{50} values were observed, as viability never dropped below 100%, implying an IC_{50} >100 µg/mL for all samples. These results confirm the safety of the macroalgae extract and CuO NPs at tested doses and highlight the nanoscaffolds' potential pro-proliferative properties, making them promising candidates for biomedical applications such as wound healing or tissue engineering. Further studies at higher concentrations (>100 µg/mL) and prolonged exposure times are recommended to establish comprehensive toxicity profiles.

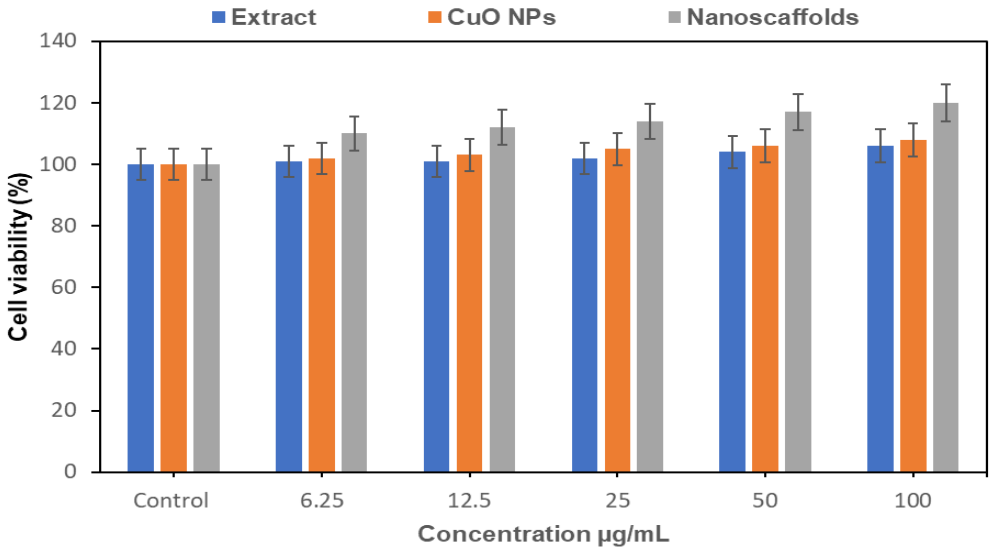

Fig. 8: Cytotoxicity analysis of algae extract, CuO NPs and nanoscaffolds

3.8. Antioxidant potential

3.8.1. DPPH Radical Scavenging Assay

The DPPH assay (Fig. 9) revealed concentration-dependent antioxidant activity across all test samples. The standard (ascorbic acid) exhibited the highest scavenging capacity, with activity increasing from 45.05% at 25 µg/mL to 89.05% at 100 µg/mL. Among the test materials, the CuO NPs-embedded starch/PVA nanoscaffolds demonstrated superior radical neutralization (42.62–86.82%) compared to bare CuO NPs (33.62–79.82%) and algal extract (22.27–73.42%). Notably, the nanoscaffolds' performance approached that of ascorbic acid at higher concentrations (100 µg/mL), suggesting enhanced electron-donating capacity due to the synergistic effects of the polymeric matrix and CuO NPs. The algal extract, while less potent, still showed significant activity, particularly at 100 µg/mL (73.42%), indicating the presence of bioactive compounds capable of hydrogen atom transfer to stabilize DPPH radicals.

3.8.2. Nitric Oxide Scavenging Assay

In the NO scavenging assay (Fig. 9), ascorbic acid again displayed the highest efficacy (35.58–84.41%), followed by the nanoscaffolds (27.62–82.82%), CuO NPs (21.62–78.82%), and algal extract (15.28–73.10%). The nanoscaffolds' superior performance may be attributed to their stabilized CuO NPs, which facilitate nitric oxide radical neutralization through redox reactions. At 100 µg/mL, the nanoscaffolds achieved 82.82% inhibition, nearing the standard's activity (84.41%), while the algal extract showed moderate scavenging, likely due to phenolic or flavonoid constituents. The results underscore the potential of nanoscaffolds as NO-scavenging agents in oxidative stress mitigation.

3.8.3. Superoxide Anion Scavenging Assay

The superoxide ($O_2^{\bullet-}$) scavenging results (Fig. 9) mirrored trends observed in other assays, with ascorbic acid (30.33–80.78%) outperforming test samples. The nanoscaffolds exhibited the highest activity among test groups (27.62–79.82%), significantly surpassing CuO NPs (21.62–69.82%) and algal extract (20.61–63.00%). The nanoscaffolds' enhanced performance may result from their structural stability, which prevents CuO NP aggregation and maintains reactive surface sites for superoxide neutralization. Notably, at 100 µg/mL, the nanoscaffolds' activity (79.82%) nearly matched the standard (80.78%), highlighting their potential as superoxide radical quenchers. The algal extract's lower efficacy suggests limited electron transfer capability compared to synthetic counterparts.

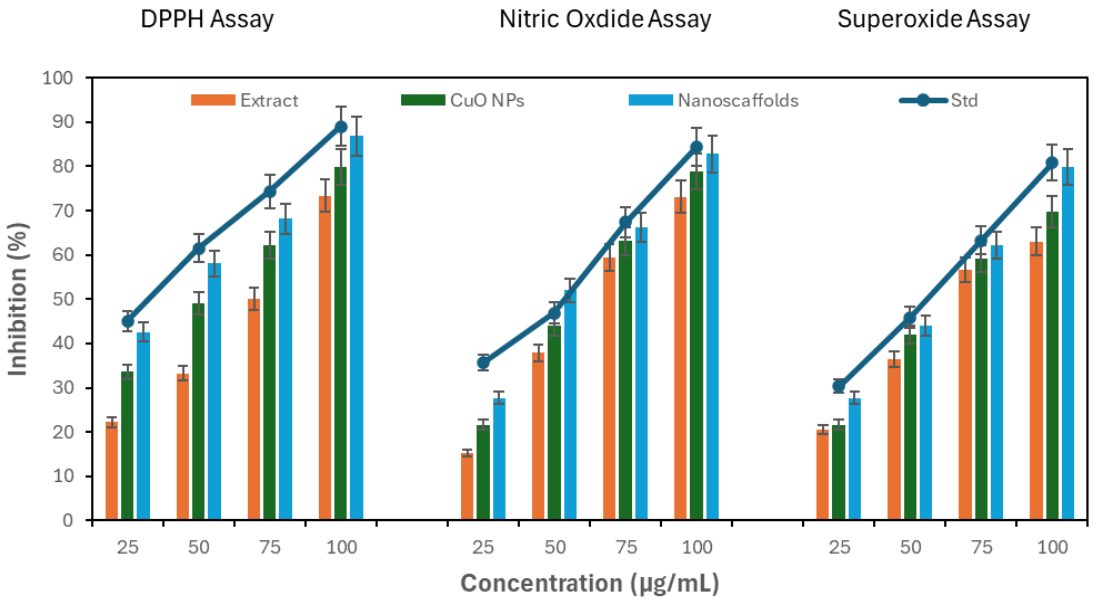

Fig. 9: Antioxidant potential of algae extract, CuO NPs and nanoscaffolds

4. DISCUSSION

The successful synthesis and characterization of CuO nanoparticles (CuO NPs) using macroalgae extract and their integration into starch/PVA electrospun nanoscaffolds have been demonstrated through a comprehensive set of analytical techniques. The findings emphasize the bioinspired, sustainable approach to nanoparticle fabrication, the physicochemical integrity of the composite scaffolds, and their potential applicability in biomedical fields.

UV–Visible Spectroscopy revealed a sharp absorption peak at 267 nm in the macroalgae extract, indicative of the presence of UV-absorbing biomolecules such as phenolic compounds and flavonoids, known for their reducing and stabilizing capabilities during green nanoparticle synthesis [20]. The CuO NP absorption peak at 292 nm, while slightly shifted from the conventional SPR range (570–600 nm for bulk CuNPs), is consistent with previously reported blue shifts in nanoparticles of reduced size or altered morphology [51-53]. This shift may result from the nanoscale dimensions, oxidation states of copper (Cu^{2+}), or strong capping interactions with phytochemicals from the macroalgae extract. The narrow and intense peak suggests a high degree of monodispersity, with minimal aggregation—a desirable property for biomedical applications such as targeted drug delivery or wound healing [54].

FTIR Spectroscopy further corroborated the involvement of bioactive compounds in CuO NP formation. Peaks corresponding to –OH, N–H, and aromatic groups indicate the presence of functional groups capable of acting as both reducing agents and stabilizers. The appearance of distinct Cu–O stretching bands between 463–672 cm^{-1} confirms successful nanoparticle synthesis [55,56]. In the composite scaffolds, overlapping peaks in the Cu–O region, shifts in –OH stretching frequencies, and emergence of a C=O band suggest effective interaction and integration of CuO NPs within the starch/PVA matrix. Such interactions may result in hydrogen bonding or esterification, enhancing the scaffold's mechanical stability and resistance to degradation—key parameters for tissue engineering matrices [57].

XRD Analysis validated the monoclinic crystalline structure of CuO NPs, with sharp, well-defined peaks matching JCPDS standards. The average crystallite size (70–90 nm), as calculated via Scherrer's equation, aligns with SEM observations and supports the high crystallinity of the biosynthesized nanoparticles. The starch/PVA scaffold demonstrated a predominantly amorphous nature, as expected due to the polymeric composition, with broad humps typical of semi-crystalline biopolymers. The retention of CuO diffraction peaks, albeit with reduced intensity, confirms the physical presence of the nanoparticles within the scaffold while suggesting a degree of encapsulation or surface coverage by the polymer network [58,59]. The observed broadening and decreased peak intensity of CuO in the composite further imply reduced nanoparticle crystallinity, likely due to polymer-induced dispersion and restriction in crystal growth—an advantage for achieving uniform distribution in drug delivery systems [60].

SEM Analysis showed that green-synthesized CuO NPs were predominantly spherical or irregular in shape, with occasional aggregation likely caused by surface charge insufficiencies. Importantly, when embedded in the starch/PVA matrix, the nanofibers retained a smooth, uniform, and bead-free morphology with an average diameter of 150–300 nm, forming a porous architecture suitable for biomedical use. The visible, evenly dispersed CuO NPs on the fiber surface suggest successful integration without compromising scaffold morphology, which is critical for applications like wound dressings, where pore interconnectivity supports cell migration and nutrient flow [61-63].

TGA demonstrated enhanced thermal stability in CuO NP-loaded scaffolds. The three-phase degradation profile (moisture loss, polymer decomposition, and carbonaceous residue breakdown) is typical for polymer composites. Notably, the delayed onset of degradation (~263°C) and high residual mass (~64%) suggest that CuO NPs act as thermal insulators or crosslinking agents, minimizing polymer chain mobility and reducing thermal decomposition. This thermal resilience expands the scaffold's applicability in scenarios requiring sterilization or mild heat processing, such as in surgical implants or wound patches [64-68].

Zeta Potential and DLS Analysis revealed that the green-synthesized CuO NPs had a moderate hydrodynamic diameter (~768 nm) and a zeta potential of -10.03 mV, indicating limited colloidal stability in aqueous dispersion. Despite this, the negative surface charge implies partial electrostatic repulsion, which can delay aggregation to some extent. The polydispersity index (0.475) suggests moderate size heterogeneity, with potential for refinement through additional surface functionalization or stabilizer optimization. These physicochemical properties are pivotal when considering in vivo applications, where stability in physiological fluids is essential [69-71].

MTT Cytotoxicity Assay clearly illustrated the biocompatibility of all tested formulations. None of the samples induced cytotoxic effects at concentrations up to 100 µg/mL, with cell viability consistently ≥100%. Interestingly, the nanoscaffolds enhanced cellular proliferation in a dose-dependent manner (up to 120% viability at 100 µg/mL), possibly due to bioactive interactions between the starch/PVA matrix and cells or the porous structure facilitating better nutrient diffusion. This mild pro-proliferative effect is particularly desirable in regenerative medicine, where scaffolds should not only be biocompatible but also promote tissue growth. The absence of IC_{50} values supports the hypothesis that these materials are safe for extended biomedical use, though further studies at higher doses and over longer durations would strengthen this conclusion [72,73].

The antioxidant evaluation of algal extract, CuO NPs, and CuO NPs-embedded starch/PVA nanoscaffolds revealed significant differences in radical scavenging capacities across DPPH, nitric oxide (NO), and superoxide

anion ($O_2^{\bullet-}$) assays, all benchmarked against ascorbic acid. The nanoscaffolds consistently exhibited superior antioxidant activity compared to bare CuO NPs and algal extract, particularly at higher concentrations (100 µg/mL), where their performance approached that of the ascorbic acid standard—reaching 86.82% (DPPH), 82.82% (NO), and 79.82% ($O_2^{\bullet-}$) scavenging. This enhanced efficacy likely stems from the synergistic interplay between the starch/PVA matrix and CuO NPs: the polymer scaffold improves nanoparticle dispersibility and stability, preventing aggregation and increasing reactive surface area for radical interaction, while the CuO NPs contribute redox-active sites for electron transfer. The algal extract, though less potent, demonstrated moderate activity (e.g., 73.42% DPPH scavenging at 100 µg/mL), attributable to natural phenolic or flavonoid constituents capable of hydrogen donation. Notably, all samples displayed dose-dependent trends, confirming classical antioxidant behavior. The nanoscaffolds' exceptional performance across multiple assays suggests their potential as multifunctional antioxidant systems, combining the advantages of biodegradable polymers (controlled release, biocompatibility) with the catalytic activity of metal nanoparticles. These findings highlight the promise of hybrid nanoscaffolds in mitigating oxidative stress, particularly in biomedical or environmental applications where sustained radical neutralization is critical. Further studies could explore mechanistic pathways, long-term stability, and in vivo efficacy to validate these materials for practical use [74].

5. CONCLUSION

In summary, this study demonstrates the green synthesis of CuO NPs using macroalgae extract and their successful incorporation into starch/PVA nanofibrous scaffolds. The physicochemical characterizations affirm the structural and thermal stability of the composites, while the biological assays confirm their biocompatibility and antioxidant efficacy. The starch-based nanoscaffold's porous morphology, thermal resilience, and pro-proliferative properties render it highly suitable for biomedical applications such as tissue engineering, wound dressing, and drug delivery platforms. Future studies should focus on in vivo biocompatibility, controlled release profiles, and long-term biodegradation kinetics to establish translational potential.

Data Availability Statement: The full dataset of physiochemical characterization associated with this work is published in Mendeley Data [Dataset] Physiochemical characterization of fabricated starch-based nanoscaffolds incorporated with *Pocockiella variegata* extract-mediated green synthesised copper oxide nanoparticles (DOI: 10.17632/6tddv74p8k.1). **Disclosure:** The material characterization data and figures (e.g., UV, SEM, FTIR, XRD, TGA, Zeta Potential and particle sizer) presented here were generated from a common dataset and are being reused across multiple related studies on nanomaterials. All biological analyses and conclusions are original to each manuscript.

Conflicts of Interest: The authors declare no conflicts of interest.

REFERENCES

[1] Daniel Raja FS, Abraham L, Rangasamy K, Saikia K, Rathankumar AK, Mironescu M, Mironescu I, Palanisamy CP, Kanniappan GV. Next-Generation Microbiome Therapeutics: Psychobiotics and Fecal Microbiota Transplants (FMT) for Mental Health Treatment. Frontiers in Cellular and Infection Microbiology. 2026; 16: 1719357.

[2] Dharmaprakash S, Gunasekaran VP, Sivaramakrishnan R, Kanniappan GV, Jayaraman S, Mironescu M, Rajabathar JR, Mironescu ID, Palanisamy CP. Marine macroalgae-mediated ultrasonic-assisted green synthesis of CuO nanoparticles embedded in starch/PVA electrospun nanoscaffolds for in vitro α-amylase and α-glucosidase inhibitory activity. Scientific Reports. 2026.

[3] Surendran N, Chandrasekaran G, Raju MV, Chandrasekaran MK, Ahalliya RM, Palanisamy CP, Kanniappan GV, Arcot R, Alharbi NS, Thiruvengadam M. Anti-inflammatory potential of ethanolic extract of Maranta arundinacea L.: Insights from COX-2 modulation and oxidative stress analysis. South African Journal of Botany. 2026; 195: 142-151.

[4] Pei J, Senthilkumar MV, Hessini K, Subramaniyam S, Sivaramakrishnan R, Kanniappan GV, Jayaraman S, Palanisamy CP. Green fabrication of starch/PVA/CuO nanoscaffolds using marine macroalgae extract for enhanced anti-inflammatory activity. Sustainable Chemistry and Pharmacy. 2026; 51: 102397.

[5] Balasubramanian V, Loganathan L, Muthuswamy K, Viswanathan TM, Raju MV, Chandrasekaran MK, Ahalliya RM, Poorasamy J, Palanisamy CP, Dominic S, Kanniappan GV. Anticancer therapeutic efficacy of PEGylated β-galactosidase from Aspergillus terreus in DMBA-induced breast cancer: Toxicological, molecular and histopathological evaluation in Wistar rats. International Journal of Biological Macromolecules. 2026; 360: 151856.

[6] Natarajan PM. Dental Bioinformnatics-Current Scope and Future perspectives. Research Journal of Pharmacy and Technology. 2022;15(5):2351-6.

[7] Natarajan PM, Umapathy VR, Murali A, Swamikannu B. (2022). Computational Simulations of Identified marine-derived Natural Bioactive Compounds As Potential Inhibitors of Oral Cancer. Future Science OA. 2022; 8(3).
[8] Natarajan PM, Umapathy VR. Role of transcriptomics in the study of oral cancer. Frontiers in Oral Health. 2025; 6:1524364.
[9] Natarajan PM, Swamikannu B, Sivaraman NM, Stylin AGSQ. Prevention of Oral Cancer: A Comprehensive Guide. Journal of Pharmacy and Bioallied Sciences. 2024; 16(5): S4239-S4241.
[10] Natarajan PM. Computational Studies on Recent Congeners of Fluoroquinolones and Nitroimidazoles for Their Use in Periodontal Therapy. Journal of Pharmacy and Bioallied Sciences. 2024; 16(5): S4731-S4740.
[11] Jayaraman S, Eswaran A, Rajagopal P, Palanisamy CP, Veerakumar P, Veeraraghavan VP, Sirasanagandla SR. Neuroendocrine-associated epigenetic factors in cellular senescence: mechanisms and therapeutic implications. Biogerontology. 2026; 27(2): 64.
[12] Ponnusamy B, Rajagopal P, Palanisamy CP, Veeraraghavan VP, Jayaraman S. Mechanistic Exploration of the anticancer activity of Justicia adhatoda Plant Leaf Ethanolic Extract against Colon Cancer Cells: An in silico and in vitro Approach. Asian Pacific Journal of Cancer Prevention. 2026; 27(3): 1069-1080.
[13] Pei J, Saran VS, Sivaramakrishnan R, Kanniappan GV, Pandurangan V, Jayaraman S, Dhayalan VK, Mironescu M, Mironescu ID, Palanisamy CP. Ultrasonic-assisted, Sargassum ilicifolium (brown marine macroalgae)-mediated biogenic synthesis of CuO nanoparticles incorporated in starch/PVA electrospun nanoscaffolds: In vitro safety and antioxidant efficacy assessment. Bioorganic Chemistry. 2026; 173: 109679.
[14] Raj MAPA, Subramaniyam S, Kanniappan GV, Jayaraman S, Palanisamy CP. Sustainable fabrication of starch/PVA/CuO electrospun nanoscaffolds from Turbinaria ornata (marine macroalgae) extract: Physicochemical characterization and antidiabetic evaluation. Kuwait Journal of Science. 2026; 53(2): 100545.
[15] Pei J, Ganesh NS, Subramaniyam S, Sivaramakrishnan R, Kanniappan GV, Jayaraman S, Palanisamy CP. Sustainable fabrication of starch/PVA/CuO electrospun nanoscaffolds from Padina tetrastromatica (Brown macroalgae) extract: Physicochemical characterization and antidiabetic assessment. Sustainable Chemistry One World. 2026; 9: 100195.
[16] Sakthiraj A, Sivaramakrishnan R, Subramaniyam S, Kanniappan GV, Pandurangan V, Jayaraman S, Dhayalan VK, Mironescu M, Mironescu ID, Palanisamy CP. Starch/PVA electrospun nanoscaffolds loaded with ultrasonic-assisted green-synthesis of CuO nanoparticles from marine macroalgae (Gracilaria corticata) extract: Cytotoxicity and antioxidant analysis. Chemical Physics Impact. 2026; 12: 101018.
[17] Raju M, Chandrasekaran MK, Loganathan L, Ahalliya RM, Mironescu M, Mironescu ID, Palanisamy CP, Kanniappan GV. Lipid remodeling and ferroptosis in phosphatidylcholine-mediated tumor–stroma crosstalk. Frontiers in Molecular Biosciences. 2026; 13: 1742305.
[18] Kunamalla R, Panagal M, Palanisamy CP. Biogenic synthesis and fabrication of starch/PVA/CuO electrospun nanoscaffolds from Sargassum ilicifolium (brown marine macroalgae) extract for anticancer activity on HT-29 and MCF-7 cancer cells. Biocatalysis and Agricultural Biotechnology. 2026; 72: 103923.
[19] Pei J, Govindaraj H, Sivaramakrishnan R, Kanniappan GV, Pandurangan V, Dhayalan VK, Mironescu M, Mironescu ID, Jayaraman S, Palanisamy PC. Sustainable fabrication of biopolymer-based (starch/PVA) nanoscaffolds loaded with green-synthesized CuO nanoparticles from Sargassum wightii (marine macroalgae): Cytocompatibility and antioxidant activity. Biomaterials Advances. 2026; 182: 214660.
[20] Pei J, Perumal NC, Meng P, Long Q, Palanisamy CP. Extracellular vesicle-based biosensors for Alzheimer's disease: A new frontier in precision diagnostics. Ageing Research Reviews. 2026; 113: 102904.
[21] Shree P, Sivaramakrishnan R, Kanniappan GV, Pandurangan V, Jayaraman S, Dhayalan VK, Mironescu M, Mironescu ID, Palanisamy CP. Antioxidant and biocompatible CuO-starch/PVA nanoscaffolds via ultrasonic green synthesis using Turbinaria conoides (brown marine macroalgae). Medicine in Drug Discovery. 2025; 28: 100238.
[22] Gong J, Lin J, Guan T, Pei J, Palanisamy CP, El-AtyFrom AMA. selenium tolerance to nanoplastic antagonism: Comprehensive characterization of L. casei SNUT1 and its extracellular vesicle–nanoselenium complex. Food Bioscience. 2025; 74: 107749.
[23] Poochi SP, Sundarraj R, Raju MV, Chandrasekaran MK, Ahalliya RM, Palanisamy CP, Kanniappan GV, Kondapavuluri BK, Thiruvengadam M. Harnessing Nature: Computational and Experimental Insights Into *Ipomoea obscura* Metabolites for Bladder Cancer Therapy. Chemistry and Biodiversity. 2025; 0: e00909.
[24] Dugganaboyana GK, Kannankumar MKG, Shivaramakrishna S, Raju MV, Chandrasekaran MK, Ahalliya RM, Panneerselvam N, Palanisamy CP, Kanniappan GV. Phytochemical insights, antioxidant activity and

therapeutic potential of Cassia senna against prostate cancer in Wistar albino rats. Discover Applied Sciences. 2025; 7:1206.
[25] Natarajan SR, Krishnamoorthy R, Alshuniaber MA, Gatasheh MK, Rajagopal P, Veeraraghavan VP, Palanisamy CP, Jayaraman S. KDM1A Facilitates Oncogenic Potential in Colorectal Cancer Progression Through the Activation of AXIN/GSK3β/β-Catenin Signaling Pathways: Evidence From Integrated Transcriptomics and In Vitro Studies. The Journal of Gene Medicine. 2025; 27(11): e70053.
[26] Natarajan PM, Bhuminathan S, Rajan R, Bindu K, Loganathan K, Veerakumar R. The Crucial Role of Smoking Cessation in Preventing Oral Cancer. Journal of Pharmacy and Bioallied Sciences. 2024; 16(5): S4245-S4247.
[27] Natarajan PM, Bhuminathan S, Leela B, Bindu K, Loganathan K, Ramachandran V. Smoking and its Role in Oral Cancer. Journal of Pharmacy and Bioallied Sciences 16(5): S4242-S4244.
[28] Vidhyarekha U, Natarajan PM, Bhuminathan S, Sabarinathan J, Suba R, Vijayalakshmi P. Role of artificial intelligence in Oral Cancer. Advances in Public Health. 2024. 2024: 3664408.
[29] Ganesan A, Kumar NG, Natarajan PM, Gauthaman J. Automated classification of elongated styloid processes using deep learning models-an artificial intelligence diagnostics. Frontiers in Oral Health. 2025; 5: 1424840.
[30] Umapathy VR, Natarajan PM, Swamikannu B. Regenerative Strategies in Dentistry: Harnessing Stem Cells, Biomaterials and Bioactive Materials for Tissue Repair. Biomolecules. 2025; 15: 546.
[31] Ganesan A, Kumar NG, Natarajan PM. Solanum trilobatum leaf extract-derived silver nanoparticles downregulate the PI3K/AKT/mTOR signaling pathway and attenuate oral squamous cell carcinoma cell proliferation. Journal of Herbmed Pharmacology. 2024; 13(2): 300-307.
[32] Perumal MKK, Renuka RR, Subbiah SK, Natarajan PM. Artificial intelligence-driven clinical decision support systems for early detection and precision therapy in oral cancer: a mini review. Frontiers in Oral Health. 2025; 6: 1592428.
[33] Ramesh E, Ganesan A, Lakshmi KC, Natarajan PM. Artificial intelligence-based diagnosis of oral leukoplakia using deep convolutional neural networks Xception and MobileNet-v2. Frontiers in Oral Health. 2025; 6: 1414524.
[34] Ganesan A, Kumar NG, Natarajan PM. Anticancer activity of silver nanoparticles synthesized from aqueous leaf extract of Solanum trilobatum (Purple fruit pea eggplant) on human oral cancer cells. Journal of Herbmed Pharmacololgy. 2024; 13(2): 260-268.
[35] Umapathy V, Dhanavel A, Kesavan R, Natarajan PM, Bhuminathan S, Vijayalakshmi P. Anticancer Potential of the Principal Constituent of Piper nigrum, Piperine: A Comprehensive Review. Cureus. 2024; 16(2): e54425.
[36] Guan T, Gong J, Lin J, Palanisamy CP, Jinjin Pei J, El-Aty AMA. Machine learning-driven multimodal optimization of selenium biotransformation and flavor profiling in fermented apple–Yacon functional beverages. Innovative Food Science & Emerging Technologies. 2025; 105: 104198.
[37] Natarajan SR, Krishnamoorthy R, Alshuniaber MA, Alsulami TS, Gatasheh MK, Rajagopal P, Palanisamy CP, Govindan R, Veeraraghavan VP, Jayaraman S. ABCE1 facilitates tumour progression via aerobic glycolysis and inhibits cell death in human colorectal cancer cells through the p53 signalling pathway. Scientific Reports. 2025; 15: 24674.
[38] Huang Y, Guo H, Liu Y, Jin W, Palanisamy CP, Pei J, Oz F, El-Aty AMA. Effects of Natural Polysaccharides on the Gut Microbiota Related to Human Metabolic Health. Molecular Nutrition & Food Research. 2025; 69:e202400792.
[39] Poornima K, Meenakshi K.C, Manikandan V.R, Shankari G, Prabhu D, Rathi M.A, Palanisamy CP, Balaji R, Gopalakrishnan V.K. Exploring the anticancer potential of Jerantinine A from *Tabernaemontana coronaria* against prostate, breast, and ovarian cancers: A computational approach. *Journal of Complementary and Integrative Medicine*, 2025 22(2): 363–372.
[40] Palanisamy CP, Poompradub S, Sansanaphongpricha K, Jayaraman S, Subramani K. Faridah Sonsudin gGreen synthesis of Nigella sativa-mediated silver nanoparticles for enhanced antibacterial activity and wound healing: Mechanistic insights and biomedical applications. Environmental Nanotechnology, Monitoring & Management. 2025; 24: 101085.
[41] Surendran N, Raju MV, Chandrasekaran MK, Ahalliya RM, Palanisamy CP, Chandrasekaran G, Kanniappan GV. Physicochemical characterization of starch from Maranta arundinacea L.(arrowroot) rhizomes and its inhibition of COX-2: In vivo validation. Bioactive Carbohydrates and Dietary Fibre. 2025; 33: 100465.

[42] Kannappan P, Chandrasekaran MK, Raju MV, Gopalakrishnan S, Dhamodharan P, Ahalliya RM, Palanisamy CP, Raju B, Kanniappan GV. Exploring the anticancer potential of Jerantinine A from Tabernaemontana coronaria against prostate, breast, and ovarian cancers: a computational approach. Journal of Complementary and Integrative Medicine. 2025; 22(02): 363-372.
[43] Pei J, Kumarasamy RV, Jayaraman S, Kanniappan GV, Long Q, Palanisamy CP. Quercetin-functionalized nanomaterials: Innovative therapeutic avenues for Alzheimer's disease management. Ageing Research Reviews. 2025; 104: 102665.
[44] Jayaraman S, Prasad M, Natarajan SR, Krishnamoorthy R, Alshuniaber MA, Gatasheh MK, Veeraraghavan VP, Rajagopal P, Palanisamy CP. Molecular mechanisms underlying the effects of beta-sitosterol on TGF-β1/Nrf2/SIRT1/p53-mediated signaling in the kidney of a high-fat diet and sucrose-induced type-2 diabetic rat. Chemico-Biological Interactions. 2025; 411: 111443.
[45] Huang Y, Guo H, Liu Y, Jin W, Palanisamy CP, Pei J, Oz F, El-Aty AMA. Effects of Natural Polysaccharides on the Gut Microbiota Related to Human Metabolic Health. Molecular Nutrition & Food Research. 2025; e202400792.
[46] Prabhakaran P, Palanisamy CP, Shanmugam A, Damodharan P, Swaminathan H, Devaraj D, Ahalliya RM, Kanniappan GV. Isolation, structural characterization, and molecular docking studies on the bioactive compound from n-Hexane extract of Emilia sonchifolia (L.) DC against the pancreatic cancer target Aurora 2 Kinase. Journal of Complementary and Integrative Medicine. 2024; 22(1): 0290.
[47] Jiang H, Kumarasamy RV, Pei J, Raju K, Kanniappan GV, Palanisamy CP. Integrating engineered nanomaterials with extracellular vesicles: Advancing targeted drug delivery and biomedical applications. Frontiers in Nanotechnology. 2024; 6: 1513683.
[48] Guo H, Liu Y, Wan T, Song D, Palanisamy CP, Geng J, Pei J, Özmen S, El-Aty AMA. Toward personalized cancer management: Role of precision nutrition–diet interventions. Journal of Functional Foods. 2024; 123: 106584.
[49] Natarajan SR, Krishnamoorthy R, Alshuniaber MA, Al-Anazi KM, Farah MA, Rajagopal P, Palanisamy CP, Veeraraghavan VP, Jayaraman S. Identification of FOXM1 as a novel protein biomarker and therapeutic target for colorectal cancer progression: Evidence from immune infiltration and bioinformatic analyses. International Journal of Biological Macromolecules. 282 (Part 4): 137201.
[50] Rajendran MS, Jayaraman S, Khan JM, Jasmine S, Prabhakaran RK, Raju MV, Chandrasekaran MK, Ahalliya RM, Kannappan P, Palanisamy CP, Kanniappan GV. Investigating the colon toxicity and carcinogenic role of monosodium glutamate compared with Dimethylhydrazine in male Wistar rats: Exploring the link to childhood colon cancer risk. Journal of King Saud University - Science. 2024; 36(11): 103507.
[51] Kumarasamy RV, Natarajan P, Umapathy VR, Roy JR, Rab SO, Saeed M, Panagal M, Mironescu M, Srinivasan GP, Palanisamy CP. Clinical Applications and Therapeutic Potentials of Advanced Nanoparticles: A Comprehensive Review on Completed Human Clinical Trials. Frontiers in Nanotechnology. 2024; 6:1479993.
[52] Jin W, Pei JJ, Roy JR, Jayaraman S, Ahalliya RM, Kanniappan GV, Mironescu M, Palanisamy CP. Comprehensive review on single-cell RNA sequencing: A new frontier in Alzheimer's disease research. Ageing Research Reviews. 2024; 274: 102454.
[53] Pei J, Palanisamy CP, Jayaraman S, Natarajan PM, Umapathy VR, Roy JR, Panagal M, Jayaraman S. Curcumin-loaded polymeric nanomaterials as a novel therapeutic strategy for Alzheimer's disease: A comprehensive review. Ageing Research Reviews. 2024; 99: 102393.
[54] Pei J, Palanisamy CP, Jayaraman S, Natarajan PM, Umapathy VR, Roy JR, Thalamati D, Ahalliya RM, Kanniappan GV, Mironescu M. A comprehensive review on starch-based Sustainable Edible Films Loaded with Bioactive Components for Food Packaging. International Journal of Biological macromolecules. 2024; 274 (Part-1): 133332.
[55] Palanisamy CP, poompradub S, Sansanaphongpricha K, Subramani K, Sonsudin F. Increased expression levels of PDGF and VEGF magnify the wound healing potential facilitated by biogenic synthesis of silver nanoparticles. Nano-Structures & Nano-Objects. 2024; 39: 101236.
[56] Pei J, Palanisamy CP, Jayaraman S, Natarajan PM, Umapathy VR, Roy JR, Thalamati D, Ahalliya RM, Kanniappan GV, Mironescu M. Proteomics Profiling of Extracellular Vesicle for Identification of Potential Biomarkers in Alzheimer's Disease: A Comprehensive Review. Ageing Research Reviews. 2024; 99: 102359.

[57] Xi J, Wang T, Xian P, Liu X, Du M, Yang H, Palanisamy CP, Lin W, Long Q. Proteomic insights uncover enhanced neurotherapeutic potential in conditioned mesenchymal stem cell-derived extracellular vesicles. Extracellular Vesicle. 2024; 3: 100037.
[58] Pei J, Natarajan PM, Umapathy VR, Swamikannu B, Sivaraman NM, Krishnasamy L, Palanisamy CP. Advancements in the synthesis and functionalization of zinc oxide-based nanomaterials for enhanced oral cancer therapy. Molecules. 2024; 29(11): 2706.
[59] Gatasheh MK, Natarajan SR, Krishnamoorthy R, Alsulami TS, Rajagopal P, Palanisamy CP, Veeraraghavan VP, Jayaraman S. Molecular analysis to identify novel potential biomarkers as drug targets in colorectal cancer therapy: an integrated bioinformatics analysis. Molecular and Cellular Oncology. 2024; 11(1): 2326699.
[60] Pei J, Yan Y, Jayaraman S, Rajagopal P, Natarajan PM, Umapathy VR, Gopathy S, Roy JR, Sadagopan CS, Thalamati D, Palanisamy CP, Mironescu M. A review on advancements in the application of starch-based nanomaterials in biomedicine: Precision drug delivery and cancer therapy. International Journal of Biological Macromolecules. 2024; 130746.
[61] Umapathy VR, Swamikannu B, Natarajan PM, Devi R, Nandini MS, Vimalarani, Vijayalakshmi P. In Silico Molecular Docking of Ocimum sanctum Phytochemicals: Targeting Key Biomarkers in Oral Cancer. Journal of Pharmacy and Bioallied Sciences. 2024; 16(5): S4792-S4799.
[62] Swamikannu B, Umapathy VR, Natarajan PM, Nandini MS, Stylin AGSQ, Vimalarani V, Rajinikanth S. Unlocking the Therapeutic Benefits of Artemisia Annua: A Comprehensive Overview of its Medicinal Properties. Journal of Pharmacy and Bioallied Sciences. 2024; 16(5): S4248-S4253.
[63] Yadalam PK, Arumuganainar D, Natarajan PM, Ardila CM. Artificial intelligence-powered prediction of AIM-2 inflammasome sequences using transformers and graph attention networks in periodontal inflammation. Scientific Reports. 2025; 15: 8733.
[64] Yadalam PK, Chatterjee S, Natarajan PM, Ardila CM. Comparison of light gradient boosting and logistic r egression for interactomic hub genes in Porphyromonas gingivalis and Fusobacterium nucleatum-induced periodontitis with Alzheimer's disease. Frontiers in Oral Health. 2025; 6:1463458.
[65] Yadalam PK, Natarajan PM, Ardila CM. Variational graph autoencoder for reconstructed transcriptomic data associated with NLRP3 mediated pyroptosis in periodontitis. Scientific Reports. 2025; 15: 1962.
[66] Pei JJ, Yan Y, Palanisamy CP, Jayaraman S, Natarajan PM, Umapathy VR, Gopathy S, Roy JR, Sadagopan JC, Thalamati D, Mironescu M. Materials-based drug delivery approaches: Recent advances and future perspectives. Green Processing and Synthesis. 2024; 13: 20230094.
[67] Pei JJ, Deng W, Liu Y, Guo Y, Chen J, Abdu H, Khan MR, Palanisamy CP, El-Aty AM. A Comprehensive Review of Cornus officinalis: Health Benefits, Phytochemistry, and Pharmacological Effects for Functional Drug and Food Development. Frontiers in Nutrition. 2023; 10: 1309963.
[68] Alugoju P, Palanisamy CP, Anthikapalli NVA, Jayaraman S, Prasanskulab A, Chuchawankul S, Dyavaiah M, Tencomnao T. Exploring the anti-aging potential of natural products and plant extracts in budding yeast Saccharomyces cerevisiae: A review. F1000Research. 2023; 12: 1265.
[69] Lavanya M, Krishnamoorthy R, Alshuniaber MA, Manoharadas S, Palanisamy CP, Veeraraghavan VP, Jayaraman S, Rajagopal P, Padmini R. Formulation, characterization and evaluation of gelatin-syringic acid/zinc oxide nanocomposite for its effective anticancer, antioxidant and anti-inflammatory activities. Journal of King Saud University-Science. 2023; 35: 102909.
[70] Palanisamy CP, Poompradub S, Sansanaphongpricha K, Jayaraman S, Subramani K, Sonsudin F. Biosynthesis of silver nanoparticles (AgNPs) using ethanolic extract of Nigella sativa (L.) seeds promotes wound healing via PDGF and VEGF signalling pathways activation. Biocatalysis and Agricultural Biotechnology. 2023; 54: 102970.
[71] Prasad M, Jayaraman S, Natarajan SR, Veeraraghavan VP, Krishnamoorthy R, Gatasheh MK, Palanisamy CP, Elrobh M. Piperine modulates IR/Akt/GLUT4 pathways to mitigate insulin resistance: Evidence from animal and computational studies. International Journal of Biological Macromolecules. 2023; 253: 127242.
[72] Palanisamy CP, Pei JJ, Phaniendra A, Venkata AAN, Jayaraman S, Veeraragahavan VP, Sridevi G, Roy JR, Janaki CS, Thalamati D, Mironescu M, Luo Q, Chai Y, Long Q. New Strategy of Neurodegenerative Disease Treatment with Extracellular Vesicles (EVs) Derived from Mesenchymal Stem Cells (MSCs). *Theranostics*. 2023; 13(12):4138-4165. doi:10.7150/thno.83066.

[73] Palanisamy CP, Phaniendra A, Jayaraman S, Poompradub S. *Nigella sativa* L. seed extracts promotes wound healing progress by activating VEGF and PDGF signalling pathways: *An in vitro* and *in silico* study. *F1000 Research*. 2023; 12: 436.

[74] Pei JJ, Palanisamy CP, Phaniendra A, Venkata AAN, Natarajan PM, Umapathy VR, Swamikannu B, Jayaraman S, Rajagopal P, Poompradub S. A comprehensive review on bio-based materials for chronic diabetic wounds. *Molecules*. 2022; 28(2), 604.